



HAL
open science

Preparation and In Vitro Validation of a Cucurbit[7]uril-Peptide Conjugate Targeting the LDL Receptor

Xue Yang, Karine Varini, Magali Godard, Fanny Gassiot, Rose Sonnette, Géraldine Ferracci, Belinda Pecqueux, Valérie Monnier, Laurence Charles, Sébastien Maria, et al.

► **To cite this version:**

Xue Yang, Karine Varini, Magali Godard, Fanny Gassiot, Rose Sonnette, et al.. Preparation and In Vitro Validation of a Cucurbit[7]uril-Peptide Conjugate Targeting the LDL Receptor. *Journal of Medicinal Chemistry*, 2023, 66 (13), pp.8844-8857. 10.1021/acs.jmedchem.3c00423 . hal-04235717

HAL Id: hal-04235717

<https://hal.science/hal-04235717v1>

Submitted on 14 Nov 2023

HAL is a multi-disciplinary open access archive for the deposit and dissemination of scientific research documents, whether they are published or not. The documents may come from teaching and research institutions in France or abroad, or from public or private research centers.

L'archive ouverte pluridisciplinaire **HAL**, est destinée au dépôt et à la diffusion de documents scientifiques de niveau recherche, publiés ou non, émanant des établissements d'enseignement et de recherche français ou étrangers, des laboratoires publics ou privés.

Preparation and *in vitro* validation of a cucurbit[7]uril-peptide conjugate targeting the LDL receptor

Xue Yang,¹ Karine Varini,² Magali Godard,² Fanny Gassiot,² Rose Sonnette,² Géraldine Ferracci,³ Belinda Pecqueux,² Valerie Monnier,⁴ Laurence Charles,¹ Sébastien Maria,¹ Micael Hardy,¹ Olivier Ouari,¹ Michel Khrestchatsky,³ Pascaline Lécorché,^{2*} Guillaume Jacquot,^{2*} David Bardelang^{1*}

¹ Aix Marseille Univ, CNRS, ICR, 13013, Marseille, France

² Vect-Horus, 13005, Marseille, France

³ Aix Marseille Univ, CNRS, INP, Inst Neurophysiopathol, 13005, Marseille, France

⁴ Aix Marseille Univ, CNRS, Centrale Marseille, FSCM, Spectropole, 13013, Marseille, France

ABSTRACT: Here we report the coupling of a cyclic peptide (VH4127) targeting the low density lipoprotein (LDL) Receptor (LDLR) *non-competitively*, to cucurbit[7]uril (CB[7]) to develop a new kind of drug delivery system (DDS), namely **CB[7]-VH4127**, with maintained binding affinity to the LDLR. To evaluate the uptake potential of this bismacrocyclic compound, another conjugate was prepared comprising a high-affinity group for CB[7] (adamantyl(Ada)-amine) coupled to the fluorescent tracker Alexa680 (A680). The resulting **A680-Ada•CB[7]-VH4127** supramolecular complex demonstrated conserved LDLR-binding potential and improved LDLR-mediated endocytosis and intracellular accumulation potential in LDLR-expressing cells. The combination of two technologies, namely mono-functionalized CB[7] and the VH4127 LDLR-targeting peptide, opens new avenues in terms of targeting and intracellular delivery to LDLR-expressing tissues or tumours. The versatile transport capacity of CB[7], known to bind a large spectrum of bioactive or functional compounds, makes this new DDS suitable for a wide range of therapeutic or imaging applications.

INTRODUCTION

Cucurbiturils, a class of synthetic macrocycles continue to attract attention.¹ In this ever growing family of host molecules,² cucurbit[7]uril (CB[7], Figure 1) has shown a series of key properties entailing researchers to actively use it in biological systems. Besides its constricted hydrophobic cavity prone to welcome a plethora of neutral or/and cationic guests with high or ultrahigh binding affinity,^{3,4} CB[7] is endowed with a good water solubility,⁵ and its low toxicity is compatible with its use in biology.⁶ Early work established the possibility to complex platinum drugs in CB[7],⁷ which was followed by numerous complexation studies^{3,4} including bioactive compounds (e. g. amantadine, camptothecin, nitidine, clofazimine, sorafenib, fasudil, arecoline),⁸ peptides,⁹ proteins,¹⁰ but also enabling to monitor enzymatic activities.¹¹ However, beside their proven ability to efficiently complex such bioactive compounds, cucurbiturils suffer from low tissue specificity. Therefore, they would benefit from conjugation to targeting ligands allowing them to drive efficient and specific delivery of therapeutic compounds to desired locations. Especially, cucurbiturils can encapsulate anticancer drugs,^{7,12} overcoming their intrinsic limitations such as: i) poor solubility, and ii) side effects,¹³ while offering at the same time two key advantages: (i) protection of the drug until reaching the site of interest and (ii) avoid unnecessary modifications of already approved drugs that often result in altered pharmacological properties. For these reasons, a drug delivery system (DDS) based on the conjugation of a targeting moiety to a cucurbituril would unlock technological

limitations in anticancer drug delivery improving both solubilization and therapeutic efficacy while minimizing side-effects.¹⁴

The chemical functionalization of CB[7] has long remained a challenge but several groups have started to report CB[7] conjugates featuring for example a PEG chain,¹⁵ fluorescent compounds,¹⁶ or DNA strands.¹⁷ The first report of a targeting CB[7] featured conjugation with biotin or an RGD peptide to target cancer cells.¹⁴ The complexation of oxaliplatin in a CB[7]-biotin conjugate resulted in enhanced *in vitro* cytotoxicity illustrating the significance and high potential of this approach.¹⁴ However, this targeting strategy based on receptor-mediated transport (RMT) does not account for reciprocal competition with the natural ligands of integrin receptors, rising questions toward competition and saturation of endogenous receptors.¹⁸ To go further, another targeting strategy relying on non-natural ligands capable of binding a receptor involved in RMT *non-competitively*, would represent a step forward.

Recently, a family of small synthetic peptide-vectors specifically targeting the Low-Density Lipoprotein (LDL) Receptor (LDLR, Figure 1a) was described, with both cross-reactive rodent/human binding potential.²⁰ Importantly, these peptides bind the LDLR at a site that does not overlap with the LDL binding site and hence does not compete with their respective binding and uptake potential, a major prerequisite to avoid any interference of LDLR function toward LDL-related biological processes.²¹ The LDLR is a high-capacity endocytic receptor, allowing efficient intracellular delivery of its ligands. This glycoprotein receptor, composed of 860 aminoacids and O-linked

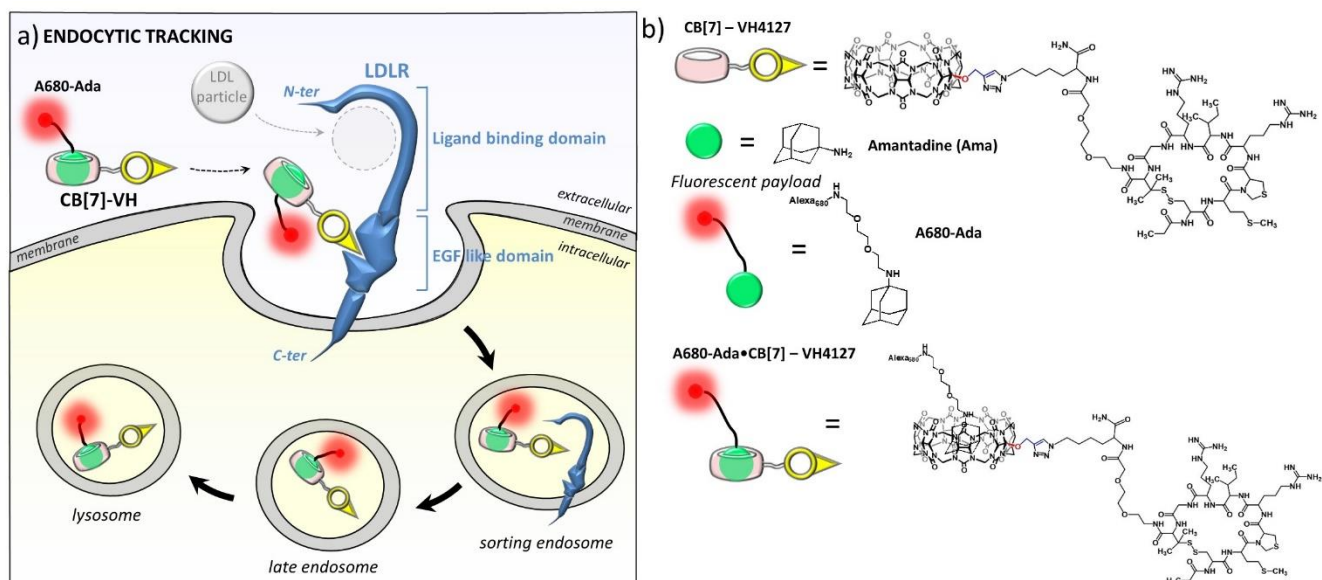


Figure 1. Concept (a) illustrating the expected *non-competitive* LDLR binding of a CB[7]-VH vector conjugate allowing cell entry of different payloads by Receptor-Mediated Transport (RMT). By binding to the EGF-like domain, the CB[7]-VH vector conjugate undergoes LDLR-mediated endocytosis as well as LDL particles, both ligands being efficiently released from LDLR in sorting endosomes and subsequently delivered in late compartments where the CB[7] guest is expected to progressively egress to the cytosol (not investigated in this work) where it can find its pharmacological target. Conversely, the LDLR is rapidly recycled from sorting endosomes back to the cell surface where it can engage new circulating ligands. Molecular structures (b) of the **CB[7]-VH4127** conjugate, of guests Amantadine (**Ama**) and Adamantane functionalized Alexa680 (**A680-Ada**) and of the **A680-Ada•CB[7]-VH4127** complex (the amine group of **A680-Ada** is considered protonated,¹⁹ the structure of Alexa680 is protected by patent and so inaccessible).

oligosaccharides is enriched in some tissues, including the liver, adrenal glands and duodenum, where it contributes to major physiological processes, including cholesterol metabolism, steroid hormone synthesis or cell growth/renewal.²² Its discovery by Brown and Goldstein led to the 1985 Nobel Prize in physiology or medicine. It is also overexpressed in many cancers where it supports rapid cell growth.²³ Therefore, LDLR represents an attractive target for many pathological conditions, including cancers, with the possibility for more efficient and specific delivery of therapeutic or imaging agents and with a better safety profile. In particular, the cyclic octapeptide **VH4127**²¹ showed high affinity toward LDLR (low nanomolar range) and high resistance to proteolytic cleavage in plasma, owing to extensive medicinal chemistry-based optimization. Not only these properties translate into high and specific LDLR-dependent intracellular accumulation potential *in vitro*^{21a} but, most importantly, lead to fast and specific distribution in LDLR-enriched tissues *in vivo*, as shown in wild-type compared to *ldlr*^{-/-} mice.^{21b,24} However, for those drugs that cannot be covalently conjugated to a molecular vector without jeopardizing their respective biological activity, the targeting potential of such peptide-vectors can be exploited by coupling them at the surface of some DDS that can complex non-covalently or encapsulate intact drugs.

Here we investigated the possibility to mono-functionalize CB[7] with the LDLR-targeting **VH4127** peptide, and the potential of this **CB[7]-VH4127** conjugate to trigger LDLR-mediated uptake of a prototypic guest in cells expressing the human LDLR (hLDLR), as shown previously with a reference Alexa680-VH4127 conjugate.^{21a} An Alexa680-Adamantane conjugate (**A680-Ada**) was used as a fluorescent guest with ultrahigh binding affinity between the Adamantane part of **A680-Ada** and the CB[7] part of **CB[7]-VH4127** for *unequivocal*

tracking along endocytic pathways (almost quantitative complexation at sub-nanomolar concentrations), a prerequisite to evaluate its potential to deliver its guest beyond early and recycling (non-productive) compartments. We show that the **CB[7]-VH4127** conjugate can be generated with acceptable yields, while keeping both LDLR-binding potential of the peptide moiety and the host•guest complexation potential of CB[7]. Importantly, the **A680-Ada•CB[7]-VH4127** supramolecular complex allowed LDLR-dependent and efficient productive uptake of the **A680-Ada** guest, with strong accumulation into late endosomal compartments of hLDLR-expressing cells.

RESULTS

Synthesis of conjugates. The **CB[7]-VH4127** conjugate was prepared after CB[7] hydroxylation under UV light,^{26,27} by functionalization with a propargyl group prior to copper click reaction with **azido-VH4127** (Figure 2 and supporting information). Briefly, CB[7] was hydroxylated²⁶ and purified by column chromatography on silica gel as previously reported to obtain several grams of monofunctional CB[7]-(OH)₁ in 20% isolated yield,²⁷ followed by a Williamson reaction with propargyl bromide to get CB[7]-(O-propargyl)₁ (60% isolated yield, Figure 2, left).²⁸ In parallel, the octapeptide sequence Pr-cM¹Thz²RLRG³Pen⁴²¹ was prepared on solid support (Figure 2, right) before cleavage of its C-terminus extremity and cyclization by mild oxidation of the two thiol groups of the cysteine and penicillamine in position 1 and 8, respectively, to generate the octapeptide Pr-[cM¹Thz²RLRG³Pen⁴]_c.²¹ The non-natural amino-acids (c: D-cysteine, Thz: thiazolidine 4-carboxylic acid and Pen: penicillamine) improve plasma stability (>4h *in-vitro* plasma half-life) and this sequence was optimized for high-affinity for LDLR.²⁴ Next, a suitable linker was added on the C-terminus. The linker was designed to be flexible and to

separate CB[7] from the vector to ensure unperturbed LDLR binding, and to carry on an azido group for subsequent coupling (Figure 2, right). To identify the best coupling conditions for the Cu(I)-catalyzed Huisgen 1,3-dipolar cycloaddition, we first investigated the conjugation between CB[7]-(O-propargyl)₁ and a model peptide **monoazido-VH4142** (structure and details in supporting information for **CB[7]-VH4142**). Finally, CB[7]-(O-propargyl)₁ was conjugated to **monoazido-VH4127** affording the **CB[7]-VH4127** conjugate in 27% isolated yield after purification by reverse-phase HPLC (Figure 2).

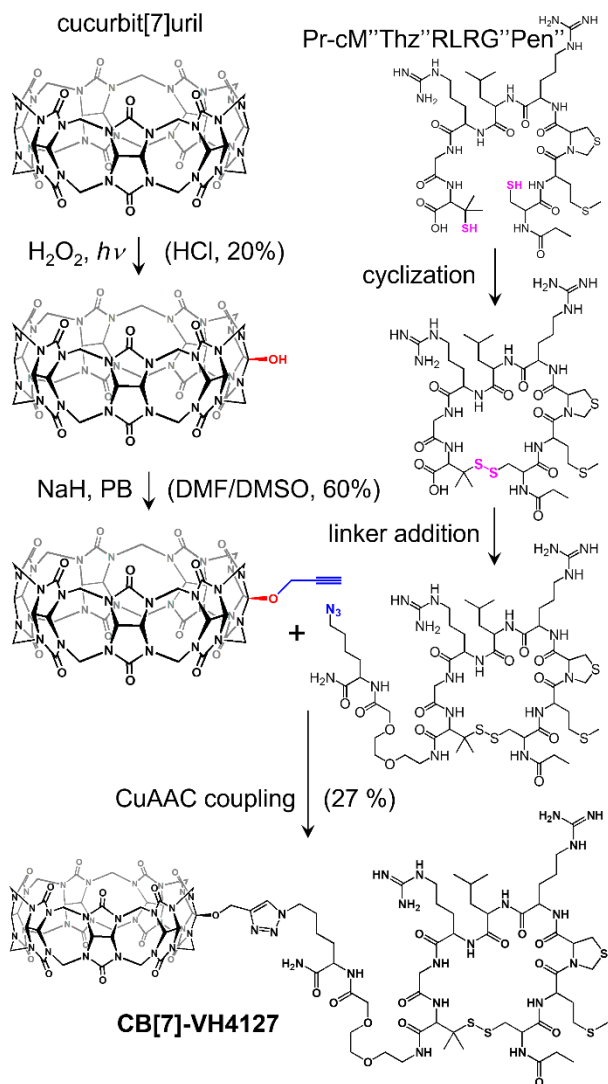


Figure 2. Synthesis of the **CB[7]-VH4127** conjugate (PB : propargyl bromide, for details see supporting information).

To efficiently monitor endocytosis, another **A680-Ada** conjugate was prepared^{16a} (see supporting information) and tested as a complex with **CB[7]-VH4127**.

LDLR binding. Binding of the **CB[7]-VH4127** conjugate to the LDL-Receptor was first evaluated by Surface Plasmon Resonance (SPR). Recombinant hLDLR-ECD (extracellular domain) was first immobilized on the surface of the sensor chip. Compounds were injected sequentially at increasing concentrations through a microflow system. Amantadine (**Ama**) was also used as a high affinity guest for the CB cavity of **CB[7]-VH4127** to

assess whether or not cavity occupancy of CB[7] would impact LDLR-binding of the **VH4127** peptide moiety. The ability of this bioactive compound to form robust host•guest complexes with CB[7], with $K_a \sim 10^{12} \text{ M}^{-1}$,^{3d,29} ensured almost quantitative complexation at sub-nanomolar concentrations, as well as for the **A680-Ada•CB[7]-VH4127** complex which remained stable after HPLC purification (no dissociation observed).

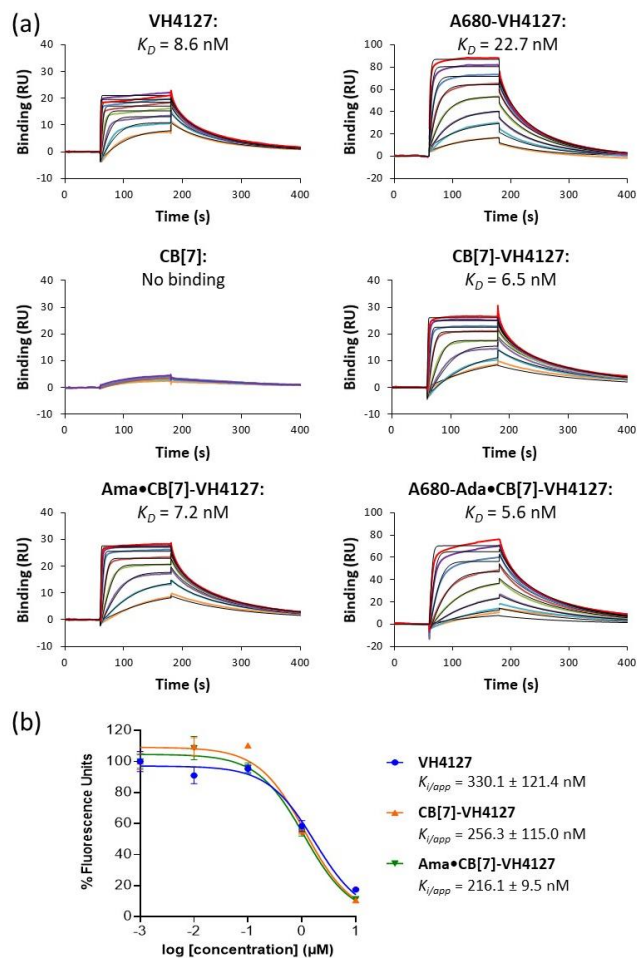


Figure 3. LDLR-binding of **VH4127** and **CB[7]-VH4127** conjugates. (a) Binding kinetics parameters (measured k_{on} /on-rate, k_{off} /off-rate and calculated K_D) on immobilized hLDLR-ECD using SPR. (b) Evaluation of hLDLR binding in living cells using a competition assay. The reference fluorescent compound AlexaFluor®680-VH4127 (**A680-VH4127**)²¹ was co-incubated at sub-saturating concentration (300 nM) with increasing concentrations of indicated compounds on CHO-hLDLR-GFP cells during 3 hours at 37°C.

CB[7]-VH4127 showed an affinity ($K_D = 6.5 \text{ nM}$, Figure 3a and Table 1) for recombinant hLDLR similar to that of free **VH4127** ($K_D = 8.6 \text{ nM}$).²¹ Measurement of binding kinetics parameters made from experimental sensorgrams (Figure 3a), namely k_{on} and k_{off} , revealed very similar values between the **CB[7]-VH4127** conjugate and the free **VH4127** peptide (Table 1).

Table 1. hLDLR-binding parameters of free **VH4127** peptide, the reference **A680-VH4127** conjugate,²¹ the **CB[7]-VH4127** conjugate and its complexes using Surface Plasmon Resonance (SPR) on immobilized hLDLR, or a competition assay in living CHO-hLDLR-GFP cells.^[a]

Compound name	Kinetic and thermodynamic parameters assessed by SPR			$K_{i/app}$ (nM)
	k_{on} (on-rate) ($M^{-1} \cdot s^{-1}$)	k_{off} (off-rate) (s^{-1})	K_D (nM)	
VH4127	$(6.59 \pm 2.77) \times 10^6$	$(4.87 \pm 1.52) \times 10^{-2}$	8.61 ± 4.09	330.1 ± 121.4
A680-VH4127	$(6.47 \pm 3.59) \times 10^5$	$(1.53 \pm 0.48) \times 10^{-2}$	22.65 ± 9.33	NA
CB[7]-VH4127	$(5.04 \pm 0.55) \times 10^6$	$(3.29 \pm 0.34) \times 10^{-2}$	6.53 ± 0.18	256.3 ± 115.0
Ama•CB[7]-VH4127	$(6.34 \pm 0.09) \times 10^6$	$(4.54 \pm 0.11) \times 10^{-2}$	7.16 ± 0.27	216.1 ± 9.5
A680-Ada•CB[7]-VH4127	$(3.94 \pm 0.13) \times 10^6$	$(2.21 \pm 0.01) \times 10^{-2}$	5.61 ± 0.17	NA

[a] SPR results are expressed as means \pm SD of 2 to 9 independent experiments. $K_{i/app}$ values obtained from competition assays are expressed as means \pm SD of n=37 independent experiments for free **VH4127**, n=3 for **CB[7]-VH4127** and n=2 for the **Ama•CB[7]-VH4127** complexed conjugate. NA: not applicable.

These results demonstrate that the conjugation of CB[7], which showed no LDLR-binding alone, to the **VH4127** peptide-vector, does not affect its LDLR-binding potential. Likewise, the presence of the guest compound **Ama** (alone or conjugated to the A680 fluorescent probe) in the CB[7] cavity, had no impact on hLDLR-binding of the complex ($K_D = 7.2$ and 5.6 nM, respectively). To confirm the LDLR binding potential of the **CB[7]-VH4127** conjugate in a cellular environment, a competition assay was performed on Chinese Hamster Ovary (CHO) cells stably expressing the hLDLR fused on its C-terminus to the Enhanced Green Fluorescent Protein (CHO-hLDLR-EGFP cells).^{21b} Briefly, this assay is based on the competition on living CHO-hLDLR-EGFP cells between a reference fluorescent compound (**A680-VH4127**, endocytic constant $K_m = 72.2$ nM in this cell line)²¹ at a fixed sub-saturating concentration of 300 nM, and the test compound (**CB[7]-VH4127**) at increasing concentrations, thereby leading to a concentration-dependent inhibition of cell-associated A680 signal quantified using flow cytometry. Fitting of the experimental data allows to determine apparent inhibition constants ($K_{i/app}$) values for each test compound (Figure 3b). Attenuation in fluorescence intensity reflects displacement of the reference peptide by the tested compounds. The curves reflect the affinity of tested compounds toward hLDLR in a competitive context and in living cells, thereby providing different, complementary information to K_D values obtained by SPR. Interestingly, **CB[7]-VH4127** and its complex with **Ama** showed very similar inhibition curves with respect to the corresponding free vector. The similar inhibition profiles and $K_{i/app}$ values found for the free **VH4127** peptide (330.1 \pm 121.4 nM), the **CB[7]-VH4127** conjugate (256.3 \pm 115.0 nM), and the **Ama•CB[7]-VH4127** complex (216.1 \pm 9.5 nM), confirmed that the presence of CB[7], loaded or not, has no impact on the LDLR-binding potential of the conjugated **VH4127** peptide on living cells.

Uptake and intracellular accumulation potential. We next investigated the LDLR-mediated intracellular delivery potential of the **CB[7]-VH4127** conjugate in the CHO-hLDLR-EGFP cell line. Of note, this cell line was previously validated for its ability to mediate LDLR-dependent uptake and intracellular delivery to late endosomal compartments of both the LDL natural ligand and the reference **A680-VH4127** conjugate.^{21a} Based on this work and that of Isaacs' and Kim's groups,^{14,16a} we prepared and used a fluorescent **A680-Ada** conjugate with ultrahigh ($10^{12} M^{-1}$) affinity for CB[7] as described for adamantane conjugates, that allowed direct detection (tracking) and quantification of the **A680-Ada•CB[7]-VH4127** complex in

cells using flow cytometry and confocal microscopy. The ultra-high affinity of this guest was used purposefully to avoid unintentional dissociation and warrant reliable fluorescent tracking along the endo-lysosomal pathways. The synthesis of **A680-Ada** and of its 1:1 complex with **CB[7]-VH4127** (Figure 1b) is described in supporting information. Before starting to assess intracellular trafficking, we first tested LDLR-binding of the **A680-Ada•CB[7]-VH4127** complex by SPR that showed an affinity for LDLR similar to that of the free **VH4127** and all other compounds carrying **VH4127** ($K_D = 5.6$ nM, Table 1, Figure 3a). We monitored endocytosis in CHO-hLDLR-EGFP cells, and tracked the distribution of the complex in live cells by confocal fluorescence microscopy with the **A680-Ada•CB[7]-VH4127** complex (Figure 4).

Based on the assays described previously, the uptake potential of the **A680-Ada•CB[7]-VH4127** complex was assessed in distinct assays in CHO-hLDLR-EGFP cells and compared to that of the reference conjugate, **A680-VH4127** (Supporting information).^{21a} First, the endocytic potential of these conjugates was compared by incubating cells during 3 hours at 37°C with increasing concentrations and the total (specific and non-specific) cellular A680-associated signal was quantified on fixed cells using flow cytometry (Figure 4a). As previously shown with the **A680-VH4127** conjugate,^{21a} both the **A680-Ada•CB[7]-VH4127** complex and the reference **A680-VH4127** conjugate showed a much higher uptake potential in hLDLR-overexpressing vs. hLDLR-negative CHO cells, with a mean 7-fold (**A680-Ada•CB[7]-VH4127** complex) and 11-fold (**A680-VH4127** conjugate) higher maximal uptake velocity V_{max} (intersection between plateau and y axis), confirming an endocytic process involving the LDLR. In addition, all uptake profiles reached a linear plateau around 300 nM, consistent with specificity and saturability of this endocytic transport system, with no or minor nonspecific uptake at higher concentrations. Interestingly, apparent K_m values, which represent ligand concentration allowing uptake at half the maximum velocity in this system, were found to be very similar between the reference **A680-VH4127** conjugate and the **A680-Ada•CB[7]-VH4127** complex (43.5 \pm 8.5 nM and 32.3 \pm 6.6 nM, respectively), suggesting similar engagement and velocity of the LDLR-mediated endocytic process. However, the **A680-Ada•CB[7]-VH4127** complex showed a mean 53% increase in the maximal uptake velocity V_{max} in hLDLR-overexpressing cells compared to the reference conjugate. Although hLDLR-negative CHO cells showed much lower uptake of both conjugates, the V_{max} of the complex was even 2.4-fold higher than

that of the reference conjugate in these cells, most likely reflecting specific and saturable uptake mediated by the low, endogenous levels of the hamster LDLR. The maximal uptake velocity V_{max} largely depends on the propensity of the ligand to dissociate from the LDLR in sorting endosomes and accumulate in late compartments, thereby allowing each LDLR molecule to

recycle back to the cell surface and take up another ligand, with hundreds of endocytosis cycles. Therefore, the higher V_{max} observed with the **A680-Ada•CB[7]-VH4127** complex suggests an unexpected higher dissociation from LDLR in sorting endosomes, resulting in a higher intracellular accumulation potential compared to the reference **A680-VH4127** conjugate.³⁰

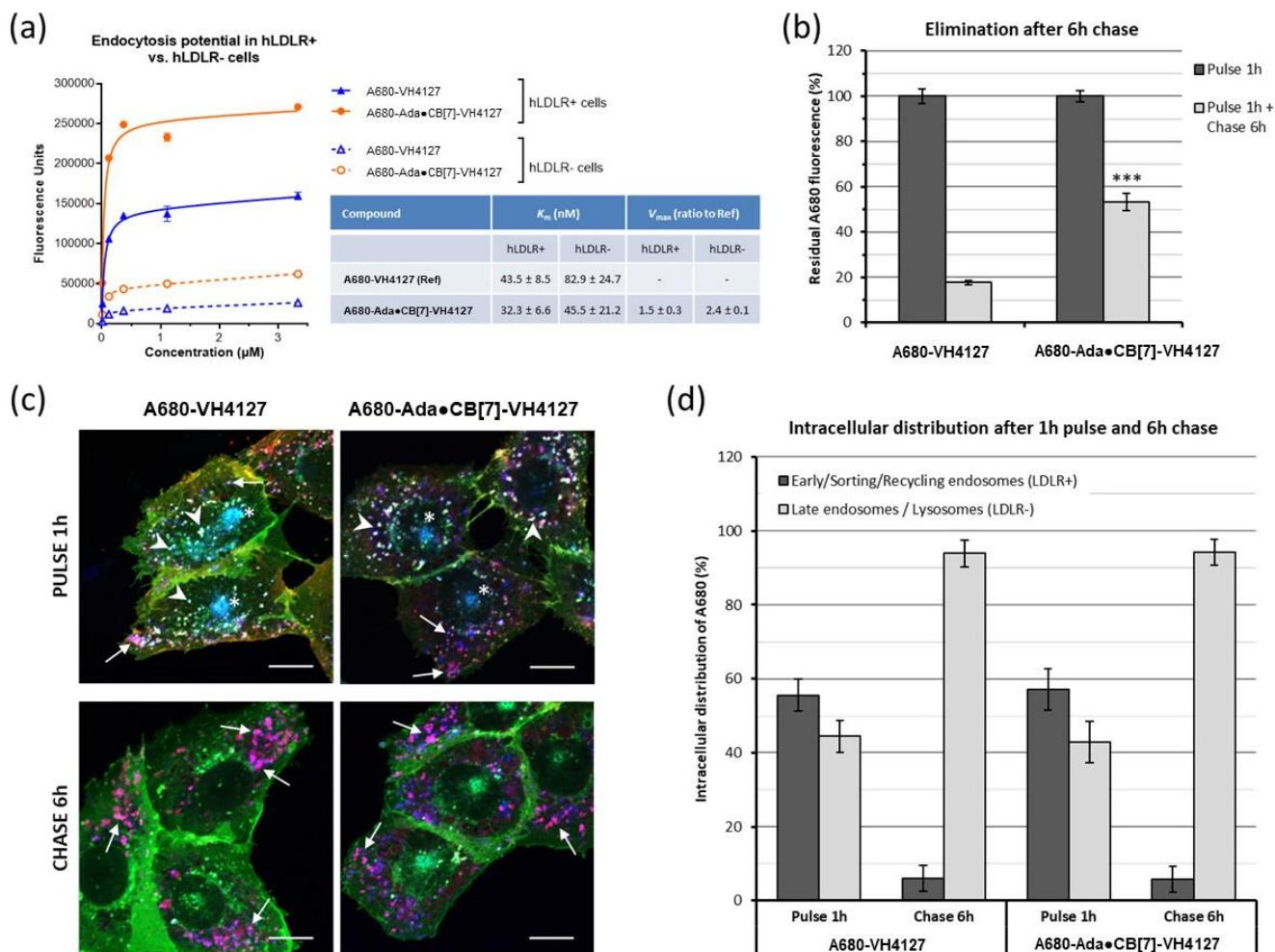


Figure 4. Uptake potential and intracellular accumulation in late compartments of the **A680-Ada•CB[7]-VH4127** complex in CHO-hLDLR-EGFP cells. (a) hLDLR-positive and control hLDLR-negative CHO cells were incubated with the indicated A680-coupled conjugates at increasing concentrations during 3 h at 37 °C. The total A680-associated signal was then quantified on fixed cells using flow cytometry. K_m and V_{max} values were estimated by fitting experimental data with a nonlinear regression. (b) Following a 1-hour incubation on CHO-hLDLR-EGFP cells of A680-coupled conjugates at the sub-saturating concentration of 300 nM (Pulse), cells were washed and then incubated for 6 hours with ligand-free medium (Chase). The residual cellular-associated A680 signal was quantified on fixed cells using flow cytometry and rationalized to the amount measured at the end of the pulse (set at 100%). Results are expressed as means ±SD. *** indicates $p < 0.001$ vs. **A680-VH4127** after 6h chase. (c) Cells were subjected to the same pulse-chase procedure (Pulse 1h / Chase 6h), except that A680-coupled conjugates were co-incubated with DiI-LDL as a marker of the LDLR-mediated endo-lysosomal pathway. Shown are representative micrographs (merged images) of fixed cells at the end of the 1 h Pulse and after 6 h Chase (hLDLR-GFP, green; DiI-LDL, red; A680-coupled vector-cargo conjugates, false blue). Arrowheads indicate LDLR- and LDL-positive early and sorting endosomes; asterisks indicate LDLR-positive and LDL-negative perinuclear endocytic recycling compartment (PERC); arrows indicate LDLR-negative and LDL-positive late compartments (late endosomes and lysosomes). Scale bars 10 μ m; (d) Quantification of intracellular distribution of A680 in either LDLR-positive (early, sorting, and recycling endosomes) or LDLR-negative (late endosomes and lysosomes) compartments.

This could be due to a unique feature of this complex, the conjugated **A680-Ada•CB[7]** complex destabilizing the ligand/receptor interface in the mild-acidic environment of sorting endosomes, where the LDLR is present in its “closed”, supposedly restrictive conformation.³¹ As shown previously using a pulse-chase procedure with similar LDLR-binding conjugates,^{21a}

evaluation of the cellular elimination profile of both conjugates allowed to estimate and compare the percentage of endocytosed molecules that readily dissociate from the LDLR in sorting endosomes and are subsequently delivered and accumulate in late compartments (late endosomes/LE and lysosomes). Using the same procedure, namely short 1-hour pulse/cellular

exposure at sub-saturating concentration as determined in previous uptake assays, followed by 6-hour chase in ligand-free medium, the extent of elimination of the **A680-Ada•CB[7]-VH4127** complex was quantified by flow cytometry (Figure 4b). As observed previously^{21a} *ca.* 80% of the reference **A680-VH4127** conjugate was eliminated from cells after 6 hours chase. This profile was shown to result from partial LDLR-

mediated recycling from endosomal compartments back to the cell surface and subsequent release in the ligand-free medium (non-productive uptake). Conclusively, the **A680-Ada•CB[7]-VH4127** complex was significantly less eliminated, with *ca.* 55% residual cellular A680-associated signal after 6 hours chase, consistent with its higher uptake and intracellular accumulation potential.

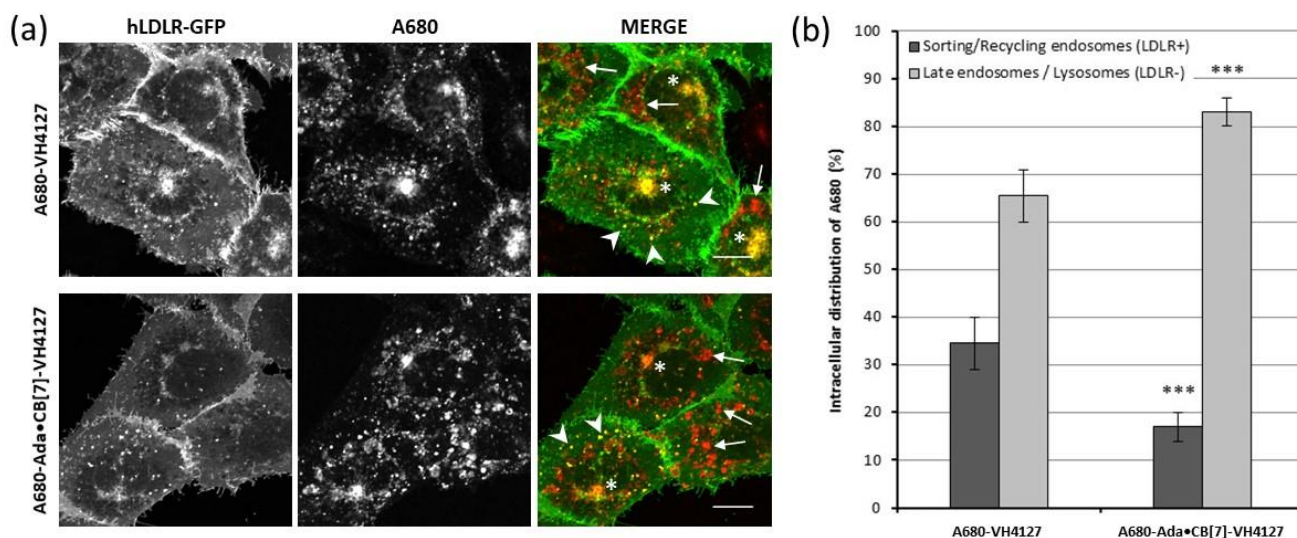


Figure 5. Intracellular distribution of **A680-VH4127** and of **A680-Ada•CB[7]-VH4127** at steady-state in CHO-hLDLR-EGFP cells. (a) Representative confocal images of fixed cells after incubation with **A680-VH4127** and **A680-Ada•CB[7]-VH4127** at non-saturating concentration (300 nM) for 6 h at 37 °C (false red color of the near-IR fluorescent dye A680). Arrowheads indicate LDLR-positive early and sorting endosomes; stars indicate LDLR-positive perinuclear endocytic recycling compartment (PERC); arrows indicate LDLR-negative late compartments (late endosomes and lysosomes). Scale bars 10 μm; (b) Quantification of intracellular distribution of A680 in either LDLR-positive (early, sorting, and recycling endosomes) or LDLR-negative (late endosomes and lysosomes) compartments, measured by the JAcOP plugin of ImageJ software ($p < 0.001$ between **A680-Ada•CB[7]-VH4127** and **A680-VH4127** in both LDLR+ or LDLR- compartments).

The intracellular distribution and fate of both conjugates was then analyzed by confocal microscopy using the same pulse-chase procedure (Figure 4d). At the end of the 1-hour pulse, both conjugates showed a rather similar co-distribution between LDLR-positive and LDLR-negative compartments, as quantified from confocal micrographs. Of note, colocalization of VH4127 conjugates with co-incubated LDL particles in early/sorting endosomes (LDLR-positive vesicles) and late compartments (LDLR-negative vesicles) confirms previous data showing the absence of competition for the uptake of both ligands of the LDLR. However, the **A680-Ada•CB[7]-VH4127** complex clearly showed a lower relative staining in the LDLR-positive perinuclear recycling compartment than the reference conjugate (asterisks in Figure 4c), indicating lower recycling to the plasma membrane and hence higher potential for delivery to late compartments. Most importantly after 6 hours chase both conjugates were mainly found in LDLR-negative and LDLR-positive compartments that were previously described as late compartments.^{21a} However, the staining intensity of cells incubated with the **A680-Ada•CB[7]-VH4127** complex was consistently brighter (lower acquisition parameters were used to get micrographs with similar intensity and quality), again indicating increased intracellular accumulation in late compartments. This was in line with the much higher residual signal as quantified in cellular elimination experiments. Finally, rationalization of the percentage of late compartment distribution after 6 hours chase (quantified from imaging experiments) to the

residual amount at the same time (quantified using flow cytometry in cellular elimination experiments) allowed to estimate the actual amount of conjugates that was readily delivered in cells (late compartments). Whereas *ca.* 17% of the reference conjugate was delivered in cells, consistent with previous findings,^{21a} this value reached *ca.* 53% for the **A680-Ada•CB[7]-VH4127** complex, definitely confirming a much better intracellular release and accumulation profile. Finally, these findings were corroborated by steady-state cellular distribution studies (6-hour continuous incubation, Figure 5). In these conditions where a distribution equilibrium is reached,^{21a} the **A680-Ada•CB[7]-VH4127** complex is distributed in significantly higher amounts in LDLR-negative late compartments than the reference conjugate (83% vs. 65%, respectively, Figure 5) which constitutes a key improvement toward an efficient LDLR-mediated DDS.

DISCUSSION

Most anticancer drugs are poorly soluble and display strong and non-specific tissue distribution *in vivo*. Hence, modifying approved drugs with suitable vectors specific to cancer tissues has been largely explored. However, chemical modifications of approved drugs are often difficult to achieve without jeopardizing their pharmacological activity. Furthermore, direct conjugation of a therapeutic entity to a molecular vector can also compromise the targeting and intracellular delivery of the latter. Thus, a versatile DDS combining (i) preserved targeting

potential and specificity, (ii) stable non-covalent drug transport and (iii) efficient intracellular drug delivery, would be highly beneficial but remains challenging. The CB[7] member of cucurbit[n]urils recently appeared as an attractive macrocyclic host with good compatibility and prerequisites for biological applications.³⁻⁶ However, beyond initial work from Isaacs' group with CB[7]-biotin,¹⁴ examples of targeted CB[7] are sparse, with either the carcinoembryonic antigen targeting M5A antibody^{32,33} or the bicyclic heptapeptide phalloidin targeting the intracellular actin.³³ Besides, none of these targeting ligands allowed receptor-mediated endocytosis of the guest•CB[7]-Ligand complex. Therefore, there remains a high need to demonstrate the feasibility to generate such a DDS able to target a cell-surface receptor and trigger efficient endocytosis and intracellular accumulation of the guest.

In this work, we explored the possibility to generate such a DDS, based on the mono-functionalization of a CB[7] macrocycle to a peptide vector efficiently targeting the LDL-receptor (LDLR), a cell-surface receptor endowed with high endocytic potential. The choice of CB[7] was based on its proven ability to form robust host•guest complexes with a wide range of bioactive or functional compounds, including anticancer drugs such as oxaliplatin, albendazole, temozolomide, irinotecan, or tamoxifen,^{7,8,14} even when CB[7] is functionalized.¹⁴ On the other hand, the rationale for using a peptide ligand targeting the LDLR with high affinity and specificity was based on the fact that this receptor displays some degree of tissue selectivity that can be leveraged for tissue-specific pathologies but also for the numerous cancers overexpressing LDLR.^{22,23} Furthermore, this cell-surface receptor is endowed with a particularly high endocytic potential, owing to its fast recycling (~10 min) and long lifespan (~20 h).³⁴ Finally, the VH4127 peptide was already validated for its potential to bind and efficiently target the LDLR in both *in vitro* and *in vivo* settings.^{21,24} This peptide also has the advantage to bind the LDLR at a region of the extracellular domain that does not overlap the LDL binding site, thereby avoiding any competitive safety issues.^{20,21} Here, we demonstrated the feasibility to conjugate this peptide to CB[7]. First, the resulting **CB[7]-VH4127** conjugate maintains its LDLR-binding potential both on the immobilized human LDLR, as assessed using Surface Plasmon Resonance, and on living cells, as assessed in a competition assay on a cell line stably expressing the human LDLR. Second, the use of a Alexa680-Adamantane (**A680-Ada**) conjugate as a prototypical fluorescent CB[7] guest allowed direct tracking and spatio-temporal evaluation of intracellular trafficking events following endocytosis in this hLDLR-expressing cell line. Not only these experiments confirmed specific and saturable LDLR-dependent uptake, as previously demonstrated with the reference **A680-VH4127** conjugate.^{21a} But they unexpectedly revealed an even higher intracellular accumulation potential of the resulting **A680-Ada•CB[7]-VH4127** complex compared to the reference conjugate, with no competition with LDL particles and co-delivery to late endosomal compartments. Although this particular behaviour remains to be fully understood, we hypothesize that it might result from a higher dissociation from LDLR than the reference **A680-VH4127** conjugate in sorting endosomes, which in turn would increase delivery to late endosomal compartments (i.e. productive uptake) rather than partial passive recycling together with the LDLR back to the cell surface (i.e. non-productive uptake).

The present work was focused on the chemical feasibility and LDLR-mediated uptake potential of a model **A680-Ada•CB[7]-VH4127** complex in an engineered cellular model overexpressing the human LDLR. Nonetheless, our results take one step

forward with the application of CB[7] targeted delivery for biological applications. First, we demonstrated here that this DDS has a particularly high LDLR-dependent intracellular accumulation potential of a CB[7] guest in LDLR-expressing cells following short, 1- to 3-hour cellular exposure. It is now of paramount importance to investigate how this feature translates in therapeutically relevant *in vitro* and *in vivo* models expressing the LDLR. As an example, this could be further investigated with new **guest•CB[7]-VH4127** complexes incorporating therapeutic or imaging agents in a model of pancreatic ductal adenocarcinoma (PDAC), as recently performed with the VH4127 peptide.³⁵ Another attractive application of the present work that is worth investigating is to use the **adamantane•CB[7]-VH4127** complex as one stand-alone versatile platform for a variety of therapeutic applications. Indeed, part of the *in vitro* validation of the LDLR-targeting DDS provided here is based on the covalent association of the Alexa680 fluorescent dye to the adamantane guest to allow investigation of its intracellular trafficking and fate. But beyond its use in the present work as a prototypical fluorescent probe, the adamantane group, which displays a remarkably high and stable affinity for CB[7],^{3d,29} can also be used as a pivotal anchor point to bioactive compounds, such as small molecules, peptides or therapeutic oligonucleotides, enabling stable association in plasma and efficient LDLR-mediated intracellular delivery of the **drug-adamantane•CB[7]-VH4127** complex in the diseased tissue. This strategy, together with the possibility to release the drug in late acidic endosomal compartments by specific cleavable linkers, is particularly appropriate when direct conjugation of the **VH4127** peptide does not afford conjugates with the desired functions. Finally, conjugation of **VH4127** to the bigger macrocycle cucurbit[8]uril (CB[8], featured by a larger cavity) could also largely expand the scope of transported bioactive compounds (i. e. steroidal hormones,^{3g} or neuromuscular block reversal agents).³⁶

CONCLUSIONS

In summary, the proposed LDLR-targeting DDS is composed of four functionally distinct parts, namely i) an LDLR-targeting peptide covalently attached to ii) the CB[7] macrocycle as a host for iii) a high affinity guest that can also act as a strong and stable anchorage point for iv) a bioactive compound (guest drug or conjugate). In the present work, we demonstrated that such DDS retained full LDLR-binding potential together with a particularly high uptake and intracellular accumulation potential in cells expressing the human LDLR of a model high affinity CB[7] guest, namely an Alexa680-Adamantane conjugate. Further work is now warranted to evaluate how this potential translates in relevant LDLR-expressing pathophysiological models, such as tumor models, for i) imaging applications and ii) therapeutic applications. This latter application will allow investigation of drug release from the CB[7] in late acidic compartments,³⁷ either passively for drugs with nanomolar affinity for the cavity of CB[7], or through specific cleavable linkers in the case of guest-drug conjugates, to escape late compartments and reach their pharmacological target. This new LDLR-targeting DDS could open a new wealth of opportunities for targeted delivery of cucurbituril•drug complexes for medical applications.

EXPERIMENTAL SECTION

General. CB[7]³⁸ and CB[7]-(OH)^{126,27} were prepared according to previous papers from our group. Alexa680-NHS (undisclosed structure) was purchased from Life Technologies (Grand Island, NY). His-tagged recombinant human LDLR

(extracellular domain, hLDLR-ECD) was purchased from Sino-Biological (Beijing, China). All other chemicals were purchased from commercial sources and used without further purification. CHO cells stand for Chinese Hamster Ovary cells. The CHO-hLDLR-EGFP cell line was engineered by Vect-Horus to stably express the human LDLR receptor tagged in C-terminal position by the GFP (Green fluorescent protein) for detection by flow cytometry and observations by microscopy.^{21a,24} CHO-hLDLR-EGFP cells were cultured in Nutrient Mix/F12 (Ham) Glutamax medium supplemented with 10% fetal calf serum, 100 U/mL penicillin, 100 µg/mL streptomycin, and 500 µg/mL Geneticin in a humidified environment at 37°C with 5% CO₂. Cell medium Nutrient Mix/F12 (Ham) Glutamax, fetal calf serum, penicillin, streptomycin, Geneticin and Dubelcco's Phosphate Buffer Saline without calcium and magnesium (D-PBS) were bought from Life Technologies (Saint Aubin, France).

NMR spectra were recorded at 300K on BRUKER Avance III nanobay – 300 or 400 spectrometers at frequencies of 300.13 MHz or 400.13 MHz respectively for ¹H and 75.46 MHz or 100.60 MHz respectively for ¹³C. Both spectrometers were equipped with a multi-nuclei 5 mm BBFO probe with Z-gradient. Splitting patterns are indicated as follows: s, singlet; d, doublet; t, triplet; m, multiplet. For CB[7]-(OH)₁ and CB[7]-(O-propargyl)₁, the spectra were recorded on the 300 or 400 MHz spectrometers using D₂O as solvent (internal reference, 4.75 ppm, and water suppress sequence when necessary). Excess cystamine (cys) was added as a guest to increase the solubility of tested compounds. For A680-Ada, the ¹H and ¹³C NMR spectra were recorded on the 300 or 400 MHz spectrometers using CDCl₃ as solvent.

For mass spectra (synthesis of CB and adamantane derivatives), a SYNAPT G2 HDMS mass spectrometer (Waters, Manchester, UK) equipped with a pneumatically assisted electrospray ionization (ESI) source was used, operated in the positive ion mode: electrospray voltage: 2.8 kV; declustering potential: 20 V; nebulization gas flow (nitrogen): 100 L/h. Mass spectra were obtained with an orthogonal acceleration time-of-flight (oa-TOF) mass analyzer. Water solution of tested samples were diluted (1/10, v/v) in methanol before analysis and then introduced in the ESI source at a 10 µL/min flow rate using a syringe pump. For HPLC-MS measurements, an ESI mass spectrometer on LCQ Fleet (ThermoFisher) was used in positive mode.

HPLC analyses of CB[7]-Peptide conjugates. Reaction progress monitoring as well as purity assessment were performed by an analytical RP-HPLC (Thermo Fisher Ultimate®3000) equipped with a Kinetex® 2.6 µm C18 100Å LC column (50×4.6 mm) using a gradient of 0% - 40% B in 10 min (UV Detection: 214 nm). The elution system consisted of solution A - H₂O (0.1% HCOOH) and solution B - acetonitrile (0.1% HCOOH) with a flow rate of 2 mL/min. The crude product was purified via preparative RP-HPLC (Thermo Fisher Ultimate®3000 series) on a Luna® 5µm C18 100Å LC column (150×10 mm). The process was monitored at 214 nm. The elution system consisted of solution A - H₂O (0.1% TFA) and solution B - acetonitrile (0.1% TFA) with a flow rate of 6 mL/min. Ratios of solutions (gradient conditions) are given hereafter. In some cases, there is a small baseline drift in HPLC traces explained by the UV wavelength we use for our analyses and the gradient system we worked with. There is an increased difference in the absorbance during the elution. Our starting system is composed of solution A which is a water solution (H₂O, 0.1% HCOOH) and gradually solution B (acetonitrile, 0.1% HCOOH) is added to solution A. However, acetonitrile absorbs more strongly than water, especially at 214 nm which is the wavelength used in our analyses. This

explains the drift observed in the baseline that we observe which is especially visible when the quantity injected is low. HPLC analyses of **A680-Ada** conjugate & **A680-Ada•CB[7]-VH4127** complex. Reaction progress monitoring and purity assessment were performed on an analytical RP-HPLC (Thermo Fisher Ultimate®3000) equipped with a Kinetex® 2.6 µm C18 100Å LC column (50×4.6 mm) using a gradient of 0% - 100% B in 10 mins (UV Detection: 214 nm and 680 nm). The elution system consisted of solution A - H₂O (0.1% HCOOH) and solution B - acetonitrile (0.1% HCOOH) with a flow rate of 2 mL/min. The crude product was purified by preparative RP-HPLC (Thermo Fisher Ultimate®3000 series) on a Luna® 5µm C18 100Å LC column (150×10 mm), monitoring at 214 nm. The elution system consisted of solution A - H₂O (0.1% TFA) and solution B - acetonitrile (0.1% TFA) with a flow rate of 6 mL/min.

Synthesis of CB[7]-(OH)₁. CB[7] (8.6 mmol, 10 g) was dissolved in a 300 mL, 10 M HCl/distilled water (1/1 v/v) solution and placed in a quartz tube before degassing with argon. After the addition of 600 µL of aqueous hydrogen peroxide (35% H₂O₂, 5.7 mmol) and stirring, the reaction mixture was irradiated with UV light (254 nm) under vigorous stirring for 5 hours and under argon. The reaction progress was monitored by ¹H-NMR of aliquots taken over time and dried before solubilization in D₂O with cystamine. The solvent was removed via rotary evaporation yielding a pale-yellow solid. The crude product composed of a mixture of CB[7]-(OH)_n (n=1-5) was purified by column chromatography on silica gel (eluent: water / acetic acid / formic acid, 10/10/2). The CB[7]-(OH)_n elute from the column in the order CB[7]-(OH)₅, CB[7]-(OH)₄, CB[7]-(OH)₃, CB[7]-(OH)₂, CB[7]-(OH)₁ and CB[7]. The solvents were removed under reduced pressure to afford 2 g of CB[7]-(OH)₁ (C₄₂H₄₂N₂₈O₁₅) as a white powder (isolated yield: 20%). Repetitive cycles of addition of cyclohexane, exposure to ultrasound and evaporation helped removing acetic acid from the product. ¹H NMR (300 MHz, D₂O) δ (ppm): 5.87 – 5.73 (m, 12H), 5.62 – 5.54 (m, 14H), 5.35 (s, 1H), 4.56 (d, *J* = 15.5 Hz, 2H expected, 0.8H observed due to watersuppress sequence), 4.34 – 4.25 (m, 12H expected, 11.2 H observed due to watersuppress sequence), consistent with literature data,³⁹ (Figure S1a). Mass spectrometry Figure S1b. HRMS (ESI) *m/z*: Calcd for C₄₆H₅₆N₃₀O₁₅S₂²⁺ ([CB[7]-(OH)₁+cys+2H]²⁺) 666.1986; Found 666.1975. Purity as assessed by ¹H NMR and mass spectrometry was >95%.

Synthesis of CB[7]-(O-propargyl)₁. CB[7]-(OH)₁ (20 mg, 17×10⁻³ mmol) was dissolved in 1.5 mL of anhydrous DMSO with the help of ultrasound and under argon before the addition of NaH (10 mg, 0.4 mmol). The reaction mixture was kept under argon and allowed to stir at room temperature for 3 hours. The reaction mixture was then cooled to 0 °C with an ice bath before the dropwise addition of propargyl bromide (0.5 mL, 4.4 mmol). The reaction mixture was further stirred overnight at room temperature under argon before addition of Et₂O to precipitate the crude product. The precipitate was isolated by centrifugation before washing the yellow solid with methanol three times. The obtained solid was dried under vacuum affording a crude product containing the targeted product and the starting product (Figure S2b). This crude product was submitted to another exactly same reaction and work-up affording 12 mg CB[7]-(O-propargyl)₁ (C₄₅H₄₄N₂₈O₁₅, Figure S2b) as an off-white powder (isolated yield: 60%). ¹H NMR (400 MHz, D₂O) δ (ppm): 5.76 – 5.62 (m, 12H), 5.54 – 5.42 (m, 14H), 5.24 (s, 1H expected, 0.36 H observed presumably due to the watersuppress sequence), 4.41 (d, *J* = 15.7 Hz, 2H expected, 1H observed due to the watersuppress sequence), 4.28 – 4.16 (m, 14H), 2.84 (s, 1H), consistent with literature data,⁴⁰ (Figure S2a). Mass

spectrometry Figure S2b. HRMS (ESI) m/z : Calcd for $C_{49}H_{58}N_{30}O_{15}S_2^{2+}$ $[[CB[7]-(O\text{-propargyl})_1+cys+2H]^{2+}]$ 685.2064; Found 685.2054.

Synthesis of Pr-VH4127-PEG₂-K(N₃)-NH₂ (VH4127: [cMThzRLRGPen]_c) and Pr-VH4142-PEG₂-K(N₃)-NH₂ (VH4142: [CMPRIRGC]_c). The peptidyl sequences H-cMThzRLRGPen-PEG₂-K(N₃)-resin and CMPRIRGC-PEG₂-K(N₃)-resin were synthesized using Fmoc SPPS methodology with an automated microwave peptide synthesizer (CEM Corporation, Matthews, NC, USA) on a Rink amide resin as previously described.²⁰ Both peptides were manually N-propionylated using a Pr₂O/DCM solution (2×5 min). After acid cleavage of the peptidyl resin with a mixture of TFA/TIS/H₂O/DTT for 2h, cyclization was performed on crude peptides by intramolecular disulfide bridge formation using K₃[Fe(CN)₆] between the first Cys or D-Cys residue and the last Cys residue. Cyclic peptides Pr-[cMThzRLRGPen]_c-PEG₂-K(N₃)-NH₂ and Pr-[CMPRIRGC]_c-PEG₂-K(N₃)-NH₂ were then purified using Reverse-Phase HPLC and their homogeneity and identity were successfully assessed by analytical LCMS using the conditions described hereafter. Instruments. HPLC: DIONEX ultimate 3000 series, column: kinetex 2.6μm C18 100A (50×4.6 mm), gradient: 10 % → 100% B, 1 to 11min, eluents: A = H₂O (HCOOH 1%) B = CH₃CN (HCOOH 1%), flow rate: 2 mL/min, UV detection: 214 nm. Mass spectrometry: LCQ Fleet ThermoFisher using positive electrospray mode. Pr-VH4127-PEG₂-K(N₃)-NH₂: Purity (HPLC-UV): 99 %, Rt = 3.47 min. Mass spectrometry: theoretical: [M+H]⁺ = 1333.60 g/mol, experimental : [M+H]⁺ = 1333.64 Da; [M+2H]²⁺ = 667.91 Da. Pr-VH4142-PEG₂-K(N₃)-NH₂: Purity (HPLC-UV): 97 %, Rt = 2.93 min. Mass spectrometry: theoretical: [M+H]⁺ = 1287.62 g/mol, experimental [M+H]⁺ = 1287.57 Da; [M+2H]²⁺ = 644.84 Da.

Synthesis of the CB[7]-VH4142 conjugate. Peptide monoazido-VH4142 ([CMPRIRGC]_c) was selected as a model peptide to optimize the coupling conditions of CB[7]-(O-propargyl)₁ with monoazido-VH4142. Based on preliminary results screening a set of reaction conditions, an excess of monoazido-peptide, of the Cu(I)•TBTA pair as a catalyst, and a short reaction time were selected as the final reaction conditions. Several stock solutions were prepared for the conjugation: (1) a CB[7]-(O-propargyl)₁ solution (2 mg/mL in distilled water); (2) a freshly prepared 100 mM CuBr solution; and (3) a 100 mM TBTA solution in DMSO/tBuOH (3/1 v/v). All the solvents were degassed by nitrogen before use. 750 μL of the CB[7]-(O-propargyl)₁ solution were added into a small glass vial containing 4.75 mg of VH4142-N₃ in 68 μL of distilled water. 50 μL of the fresh CuBr solution were mixed with 50 μL of the TBTA solution to prepare the Cu(I)/ligand solution which was subsequently added to the cucurbituril/peptide solution thereby starting the coupling reaction that proceeded at room temperature for 15 minutes under stirring. Reaction progress was monitored by analytical RP-HPLC. The crude product was then purified by preparative RP-HPLC (Table S1). Purity and characterization of the obtained CB[7]-VH4142 conjugate were assessed by analytical RP-HPLC and ESI mass spectrometry on LCQ Fleet (ThermoFisher) used in positive mode (Figure S3). Yield: 39%; Purity: 97%.

Synthesis of the CB[7]-VH4127 conjugate. Based on the experience gained using monoazido-VH4142, optimized conditions for the CuAAC reaction were used for the conjugation of monoazido-VH4127 ([cMThzRLRG"Pen"]_c) with CB[7]-(O-propargyl)₁. Several stock solutions were prepared for the conjugation: (1) a CB[7]-(O-propargyl)₁ solution (2 mg/mL in distilled water); (2) a freshly prepared 100 mM CuBr solution; and (3) a 100 mM TBTA solution in DMSO/tBuOH (3/1 v/v). All the

solvents were degassed by nitrogen before use. For peptide stereochemistry, see Figure 2 of the paper. 1050 μL of the CB[7]-(O-propargyl)₁ solution were added into a small glass vial containing 6.6 mg of VH4127-N₃ in 75 μL of distilled water. 68 μL of the fresh CuBr solution were mixed with 68 μL of the TBTA solution to prepare the Cu(I)/ligand solution which was subsequently added to the cucurbituril/peptide solution thereby starting the coupling reaction that proceeded at room temperature for 15 mins. Reaction progress was monitored by analytical RP-HPLC. The crude product was then purified by preparative RP-HPLC (Table S2). Purity and characterization of the obtained CB[7]-VH4127 conjugate were assessed by analytical RP-HPLC and ESI mass spectrometry on LCQ Fleet (ThermoFisher) used in positive mode (Figure S4). Yield: 27%; Purity 99%.

Synthesis of the A680-Ada conjugate. A680 NHS-ester (2 mg, Life Technologies, structure patented) was first dissolved in 60 μL of DMF and *N*-(2-(2-(2-aminoethoxy)ethoxy)ethyl)adamantan-1-amine (18.36 mg, preparation in supporting information) was dissolved in 500 μL of DMF. The amine solution (8.2 μL, 1 μmol, 1 equiv.) was introduced in 0.5 mL of DMF, together with the A680 NHS-ester solution (36 μL, 1.2 mg) and 1.5 equiv. of DIEA, before stirring at room temperature for 15 minutes. Reaction progress was monitored by analytical RP-HPLC. The crude product was then purified by preparative RP-HPLC (Table S3). Because the molecular weight of A680 NHS-ester is unknown, the molecular weight of purified A680-Ada was confirmed approximately by ESI mass spectrometry and the purity was assessed by analytical RP-HPLC (Figure S8). Yield: 25.5%; Purity 99%.

Preparation of the A680-Ada•CB[7]-VH4127 complex. To avoid fluorescence interferences that could come from non-complexed A680-Ada during confocal microscopy, an exact 1:1 A680-Ada•CB[7]-VH4127 complex was required. CB[7]-VH4127 and A680-Ada were first dissolved in distilled water to prepare stock solutions. The two solutions were then mixed assuming a calculated 1:1 host-guest ratio. HPLC-MS was used to check formation of the complex. Instead of the expected single peak corresponding to the desired complex, two peaks were observed on chromatograms, corresponding to the desired A680-Ada•CB[7]-VH4127 complex and to free A680-Ada (Figure S9). The fraction corresponding to the complex was collected and analyzed again by HPLC-MS to check if this result could have been caused by an instability of the complex in the conditions of HPLC-MS. The single peak for the complex observed on this chromatogram excluded this possibility. We thus decided to iteratively add more CB[7]-VH4127 up to the total disappearance of the peak corresponding to A680-Ada. This process was followed by HPLC (Figure S10) and the ratio of the two compounds to produce the desired complex was CB[7]-VH4127 : A680-Ada = 1.6 : 1. Then the mixture was purified by preparative RP-HPLC (Table S4) and the desired 1:1 A680-Ada•CB[7]-VH4127 complex was obtained. The purified complex was further identified by analytical RP-HPLC and ESI mass spectrometry (Figure S11). Purity: 99%.

Surface Plasmon Resonance (SPR). The association rate constant (on-rate, k_{on}) and dissociation rate constant (off-rate, k_{off}) of our tested compounds toward LDLR have been measured by SPR. Their ratio gives access to the equilibrium dissociation constant K_D ($K_D = k_{off}/k_{on}$) which is related to the conjugate's binding affinity toward LDLR. SPR measurements were performed at 25°C using a Biacore T200 apparatus (Cytiva) and 50 mM HEPES-NaOH pH 7.4, 150 mM NaCl, 0.005% Tween-20 (v/v) as running buffer. The His-tagged recombinant extracellular domain of the human LDL-receptor (hLDLR-ECD,

SinoBiological, Beijing, China) was immobilized on HC1500m sensorchips (Xantec, Dusseldorf, Germany) by amine coupling at pH 5, according to manufacturer's instruction, at a density of around 125 fmol/mm². A flow cell with an irrelevant protein, the SNAP25 (Synaptosomal-Associated Protein, 25kDa) coupled at pH 4 at the same density was used as control flow cell. Different concentrations of the analytes (5-640 nM for **VH4127**, **Ama•CB[7]-VH4127** and **A680-Ada•CB[7]-VH4127**; 10-1280 nM for **CB[7]-VH4127**) were prepared by two-fold dilutions in running buffer and injected over the flow cells during 120 seconds at 30 μ L/min with a dissociation time of 600 seconds. Complete dissociation allowed analysis without regeneration. Blank runs of running buffer were performed in the same condition. *Coloured lines of Figure 3*: experimental specific binding curves of molecules at each test concentration obtained after double subtraction of the signal measured on the control flow cell (without immobilized LDLR) and a blank run. *Black lines*: fit curves of the experimental data with a kinetic titration 1:1 Langmuir interaction model using Biacore T200 Evaluation version 2.0 software. Data shown are representative of 2 to 6 independent experiments.

Competition assay in live cells. On-cell competition assay was used to determine apparent inhibition constant ($K_{i/app}$) values from inhibition curves for each tested compound on CHO-hLDLR-EGFP cells. The reference fluorescent compound AlexaFluor[®]680-VH4127 (**A680-VH4127**),^{21a} which is of known affinity for hLDLR, was prepared previously and used for the measurements. Cells were plated in a 96-well microplate and exposed to increasing concentrations of tested compounds (**VH4127**, **CB[7]-VH4127** and the **Ama•CB[7]-VH4127** complex: 0.001, 0.01, 0.1, 1, and 10 μ M) in the presence of the reference compound **A680-VH4127** at a sub-saturating concentration of 300 nM for 3 h at 37 °C. After treatment, cells were washed by D-PBS and dissociated by incubating with Trypsin/EDTA for 5 mins at 37 °C, before the addition of cold culture media (4 °C) to stop the action of Trypsin. Resuspended cells were transferred in a 96-deepwell plate containing 1% SVF 0.02% sodium azide in PBS and then centrifuged for 5 min at 2000 rpm at 4 °C. After removing supernatant, 5 mM EDTA in D-PBS and 4% paraformaldehyde (PFA) (v/v 1:1) were added into wells to fix cells for 10 min at room temperature. PFA was removed by centrifugation (5 min, 2000 rpm) and cells were resuspended with 5 mM EDTA in D-PBS. Then the cellular A680-associated fluorescent signals was quantified using an Attune[™] NxT flow cytometer (Thermo Fisher Scientific) equipped with Attune[™] NxT v3.1.2. Inhibition curves were fitted with GraphPad Prism[®] software using a nonlinear fit to get the $K_{i/app}$ values.

Evaluation of endocytic constant K_m and maximal uptake velocity (V_{max} , Figure 4a). Sub-confluent CHO-hLDLR-GFP cells or CHO cells in 96-well plates were incubated with **A680-VH4127** and **A680-Ada•CB[7]-VH4127** at increasing concentrations for 3 h at 37 °C. After the completion of incubation, the total cellular A680-associated fluorescent signals were quantified via flow cytometry (cells were prepared for the flow cytometry assay in the same way as the method in the 'competition assay in live cells' section). Experimental data (means \pm SD) were fit with a nonlinear regression (solid lines) using GraphPad Prism[®] software to estimate K_m and V_{max} values. The value of the endocytic constant K_m corresponds to the concentration of tested compounds allowing their binding and endocytosis at half-maximal velocity of hLDLR in this cellular model and the maximal velocity V_{max} value represents the maximum uptake potential of tested compounds.

Evaluation of cellular elimination. Total cellular elimination of A680-coupled vector-cargo conjugates was studied on sub-confluent CHO-hLDLR-GFP cells grown in 48-well plates using a pulse-chase protocol (1-hour pulse followed by chase in ligand-free medium during 6 h). Both **A680-VH4127** and **A680-Ada•CB[7]-VH4127** were incubated at the sub-saturating concentration of 300 nM (selected based on previous uptake/ K_m experiments). At the end of the pulse or after an additional 6-hour chase, the total cellular A680-associated fluorescent signals were quantified via flow cytometry (cells were prepared for the flow cytometry assay in the same way as the method in the 'competition assay in live cells' section). The residual amount of A680-coupled vector-cargo conjugates at the end of the pulse-chase procedure was calculated as a ratio to the total A680-associated signal measured at the end of the pulse (set at 100%).

Evaluation of steady-state intracellular distribution (Figure 5). CHO-hLDLR-GFP cells grown onto glass coverslips in 24-well plates were incubated with **A680-VH4127** and **A680-Ada•CB[7]-VH4127** at the non-saturating concentration of 300 nM for 6 h at 37 °C. At the end of incubation, cells were washed with cold D-PBS for 3 times and then fixed by 4% PFA for 10 min at room temperature. Nuclei were stained with Hoechst 1:1000 solution (Hoechst staining not shown in Figure 5). Coverslips containing cells were mounted on glass slides in Prolong Gold after washing by PBS for 3 times. Images were acquired using a laser-scanning confocal microscope (LSM700, Zeiss) equipped with Zen 2012 software. Each fluorophore was imaged sequentially. JACoP plugin of ImageJ software was employed to quantify the intracellular distribution of A680 in either LDLR-positive (early, sorting, and recycling endosomes) or LDLR-negative (late endosomes and lysosomes) compartments. Ten full images (up to five cells in one image) were analyzed for each group.

ASSOCIATED CONTENT

Supporting Information.

NMR and mass spectra of synthesized compounds and HPLC-MS analyses of the conjugates, **CB[7]-VH4142**, **CB[7]-VH4127**, **A680-Ada** and of the complex **A680-Ada•CB[7]-VH4127** can be found in the supporting information. This material is available free of charge via the Internet at <http://pubs.acs.org>.

AUTHOR INFORMATION

Corresponding Authors

Pascaline Lecorche – Vect-Horus, Marseille, France; Email: pascaline.lecorche@vect-horus.com

Guillaume Jacquot – Vect-Horus, Marseille, France; Email: guillaume.jacquot@vect-horus.com

David Bardelang - Aix Marseille Univ, CNRS, ICR, Marseille, France; Email: david.bardelang@univ-amu.fr

Authors

Xue YANG and Karine VARINI contributed equally to this work.

Xue Yang - Aix Marseille Univ, CNRS, ICR, 13013, Marseille, France

Karine Varini - Vect-Horus, 13005, Marseille, France

Magali Godard - Vect-Horus, 13005, Marseille, France

Fanny Gassiot - Vect-Horus, 13005, Marseille, France

Rose Sonette - Vect-Horus, 13005, Marseille, France

Géraldine Ferracci – Aix-Marseille Univ, CNRS, INP, Inst Neurophysiopathol, 13005, Marseille, France

Belinda Pecqueux - Vect-Horus, 13005, Marseille, France

Valérie Monnier - Aix Marseille Univ, CNRS, Centrale Marseille, FSCM, Spectropole, 13013, Marseille, France

Laurence Charles - Aix Marseille Univ, CNRS, ICR, 13013, Marseille, France

Sébastien Maria - Aix Marseille Univ, CNRS, ICR, 13013, Marseille, France

Micael Hardy - Aix Marseille Univ, CNRS, ICR, 13013, Marseille, France

Olivier Ouari - Aix Marseille Univ, CNRS, ICR, 13013, Marseille, France

Michel Khrestchatsky – Aix-Marseille Univ, CNRS, INP, Inst Neurophysiopathol, 13005, Marseille, France

Notes

The authors declare no competing financial interest.

ACKNOWLEDGMENT

CNRS, Aix Marseille Université and the VECT-HORUS biotech company are acknowledged for continuous support. This project has received funding from the European Union's Horizon 2020 research and innovation programme under the Marie Skłodowska-Curie grant agreement No. 713750. Also, it has been carried out with the financial support of the Regional Council of Provence-Alpes-Côte d'Azur and with the financial support of the A*MIDEX (no. ANR-11- IDEX-0001-02), funded by the Investissements d'Avenir project funded by the French Government, managed by the French National Research Agency (ANR). We also warmly thank Pr. Ruibing Wang (University of Macau) and Pr. Andreas Hennig (Osnabruck University) from helpful discussions about CB[7]-(OH)₁ propargylation.

REFERENCES

- (1) (a) An, J.; Kim, S.; Shrinidhi, A.; Kim, J.; Banna, H.; Sung, G.; Park, K. M.; Kim, K. Purification of protein therapeutics via high-affinity supramolecular host-guest interactions, *Nat. Biomed. Eng.* **2020**, *4*, 1044–1052. (b) Pazos, E.; Novo, P.; Peinador, C.; Kaifer, A. E.; Garcia, M. D., Cucurbit[8]uril (CB[8])-Based Supramolecular Switches, *Angew. Chem., Int. Ed.* **2019**, *58*, 403–416. (c) Sokolowski, K.; Huang, J.; Földes, T.; McCune, J. A.; Xu, D. D.; de Nijs, B.; Chikkaraddy, R.; Collins, S. M.; Rosta, E.; Baumberg, J. J.; Scherman, O. A. Nanoparticle surfactants for kinetically arrested photoactive assemblies to track light-induced electron transfer, *Nat. Nanotech.* **2021**, *16*, 1121–1129. (d) Deng, C.-L.; Murkli, S. L.; Isaacs, L. D. Supramolecular hosts as in vivo sequestration agents for pharmaceuticals and toxins, *Chem. Soc. Rev.* **2020**, *49*, 7516–7532. (e) He, S.; Biedermann, F.; Vankova, N.; Zhechkov, L.; Heine, T.; Hoffman, R. E.; De Simone, A.; Duignan, T. T.; Nau, W. M., Cavitation energies can outperform dispersion interactions, *Nat. Chem.* **2018**, *10*, 1252–1257.
- (2) (a) Lee, J. W.; Samal, S.; Selvapalam, N.; Kim, H.-J.; Kim, K., Cucurbituril Homologues and Derivatives: New Opportunities in Supramolecular Chemistry, *Acc. Chem. Res.* **2003**, *36*, 621–630. (b) Lagona, J.; Mukhopadhyay, P.; Chakrabarti, S.; Isaacs, L., The cucurbit[n]uril family, *Angew. Chem., Int. Ed.* **2005**, *44*, 4844–4870. (c) Barrow, S. J.; Kasper, S.; Rowland, M. J.; del Barrio, J.; Scherman, O. A., Cucurbituril-based molecular recognition, *Chem. Rev.* **2015**, *115*, 12320–12406. (d) Assaf, K. I.; Nau, W. M., Cucurbiturils: from synthesis to high-affinity binding and catalysis, *Chem. Soc. Rev.* **2015**, *44*, 394–418. (e) Masson, E.; Ling, X.; Joseph, R.; Kyeremeh-Mensah, L.; Lu, X., Cucurbituril chemistry: a tale of supramolecular success, *RSC Adv.* **2012**, *2*, 1213–1247.
- (3) (a) Barbero, H.; Masson, E. Design and recognition of cucurbituril-secured platinum-bound oligopeptides, *Chem. Sci.* **2021**, *12*, 9962–9968. (b) Neira, I.; García, M. D.; Peinador, C.; Kaifer, A. E. Cucurbiturils as Effectors on the Self-Assembly of Pd(II) and Pt(II) Metallacycles, *J. Org. Chem.* **2021**, DOI: 10.1021/acs.joc.1c01460. (c) Palma, A.; Artelsmair, M.; Wu, G.; Lu, X.; Barrow, S. J.; Uddin, N.; Rosta, E.; Masson, E.; Scherman, O. A. Cucurbit[7]uril as a Supramolecular Artificial Enzyme for Diels–Alder Reactions, *Angew. Chem. Int. Ed.* **2017**, *56*, 15688–15692. (d) Liu, S.; Ruspici, C.; Mukhopadhyay, P.; Chakrabarti, S.; Zavalij, P. Y.; Isaacs, L., The Cucurbit[n]uril Family: Prime Components for Self-Sorting Systems, *J. Am. Chem. Soc.* **2005**, *127*, 15959–15967. (e) Jiao, Y.; Tang, B.; Zhang, Y.; Xu, J.-F.; Wang, Z.; Zhang, X. Highly Efficient Supramolecular Catalysis by Endowing the Reaction Intermediate with Adaptive Reactivity, *Angew. Chem. Int. Ed.* **2018**, *57*, 6077–6081. (f) Tang, H.; Fuentealba, D.; Ko, Y. H.; Selvapalam, N.; Kim, K.; Bohne, C. Guest Binding Dynamics with Cucurbit[7]uril in the Presence of Cations, *J. Am. Chem. Soc.* **2011**, *133*, 20623–20633. (g) Lazar, A. I.; Biedermann, F.; Mustafina, K. R.; Assaf, K. I.; Hennig, A.; Nau, W. M. Nanomolar Binding of Steroids to Cucurbit[n]urils: Selectivity and Applications, *J. Am. Chem. Soc.* **2016**, *138*, 13022–13029. (h) Yang, X.; Cheng, Q.; Monnier, V.; Charles, L.; Karoui, H.; Ouari, O.; Gimes, D.; Wang, R.; Kermagoret, A.; Bardelang, D. Guest exchange by a partial energy ratchet in water, *Angew. Chem. Int. Ed.* **2021**, *60*, 6617–6623.
- (4) (a) Rekharsky, M. V.; Mori, T.; Yang, C.; Ko, Y. H.; Selvapalam, N.; Kim, H.; Sobransingh, D.; Kaifer, A. E.; Liu, S.; Isaacs, L.; Chen, W.; Moghaddam, S.; Gilson, M. K.; Kim, K.; Inoue, Y., A synthetic host-guest system achieves avidin-biotin affinity by overcoming enthalpy-entropy compensation, *Proc. Natl. Acad. Sci. USA* **2007**, *104*, 20737–20742. (b) Cao, L.; Sekutor, M.; Zavalij, P. Y.; Mlinaric-Majerski, K.; Glaser, R.; Isaacs, L., Cucurbit[7]uril Guest Pair with an Attomolar Dissociation Constant, *Angew. Chem., Int. Ed.* **2014**, *53*, 988–993. (c) Shetty, D.; Khedkar, J. K.; Park, K. M.; Kim, K. Can we beat the biotin-avidin pair?: cucurbit[7]uril-based ultrahigh affinity host-guest complexes and their applications, *Chem. Soc. Rev.* **2015**, *44*, 8747–8761.
- (5) (a) Mikulu, L.; Michalicova, R.; Iglesias, V.; Yawer, M. A.; Kaifer, A. E.; Lubal, P.; Sindelar, V. pH Control on the Sequential Uptake and Release of Organic Cations by Cucurbit[7]uril, *Chem. Eur. J.* **2017**, *23*, 2350–2355. (b) Jiao, D.; Zhao, N.; Scherman, O. A. A “green” method for isolation of cucurbit[7]uril via a solid state metathesis reaction, *Chem. Commun.* **2010**, *46*, 2007–2009. (c) Cong, H.; Ni, X. L.; Xiao, X.; Huang, Y.; Zhu, Q.-J.; Xue, S.-F.; Tao, Z.; Lindoy, L. F.; Wei, G. Synthesis and separation of cucurbit[n]urils and their derivatives, *Org. Biomol. Chem.* **2016**, *14*, 4335–4364. (d) Ong, W.; Gómez-Kaifer, M.; Kaifer, A. E. Cucurbit[7]uril: A Very Effective Host for Viologens and Their Cation Radicals, *Org. Lett.* **2002**, *4*, 1791–1794. (e) Yin, H.; Rosas, R.; Gimes, D.; Ouari, O.; Wang, R.; Kermagoret, A.; Bardelang, D. Metal actuated ring translocation switches in water, *Org. Lett.* **2018**, *20*, 3187–3191. (f) Wang, H.; Yan, Y.-Q.; Yi, Y.; Wei, Z.-Y.; Chen, H.; Xu, J.-F.; Wang, H.; Zhao, Y.; Zhang, X. Supramolecular Peptide Therapeutics: Host-Guest Interaction-Assisted Systemic Delivery of Anticancer Peptides, *CCS Chem.* **2020**, *2*, 739–748.
- (6) Uzunova, V. D.; Cullinane, C.; Brix, K. Nau, W. M.; Day, A. I. Toxicity of cucurbit[7]uril and cucurbit[8]uril: an exploratory in vitro and in vivo study, *Org. Biomol. Chem.* **2010**, *8*, 2037–2042. (b) Hettiarachchi, G.; Nguyen, D.; Wu, J.; Lucas, D.; Ma, D.; Isaacs, L.; Briken, V. Toxicology and Drug Delivery by Cucurbit[n]uril Type Molecular Containers, *Plos One* **2010**, *5*, e10514. (c) Chen, H.; Chan, J. Y. W.; Yang, X.; Wyman, I. W.; Bardelang, D.; Macartney, D. H.; Lee, S. M. Y.; Wang, R. Developmental and organ-specific toxicity of cucurbit[7]uril: in vivo study on zebrafish models, *RSC Adv.* **2015**, *5*, 30067–30074. (d) Zhang, X.; Xu, X.; Li, S.; Wang, L.-H.; Zhang, J.; Wang, R. A systematic evaluation of the biocompatibility of cucurbit[7]uril in mice, *Sci. Report* **2018**, *8*, 8819.
- (7) (a) Wheate, N. J.; Day, A. I.; Blanch, R. J.; Arnold, A. P.; Cullinane, C.; Collins, J. G. Multi-Nuclear Platinum Complexes Encapsulated in Cucurbit[n]uril as an Approach to Reduce Toxicity in Cancer Treatment, *Chem. Commun.* **2004**, 1424–1425. (b) Jeon, Y. J.; Kim, S.-Y.; Ko, Y. H.; Sakamoto, S.; Yamaguchi, K.; Kim, K. Novel Molecular Drug Carrier: Encapsulation of Oxaliplatin in Cucurbit[7]uril and its Effects on Stability and Reactivity of the Drug, *Org.*

- Biomol. Chem.* **2005**, *3*, 2122–2125. (c) Wheate N. J.; Improving platinum(II)-based anticancer drug delivery using cucurbit[n]urils, *J. Inorg. Biochem.* **2008**, *102*, 2060–2066.
- (8) (a) Das, D.; Assaf, K. I.; Nau, W. M. Applications of Cucurbiturils in Medicinal Chemistry and Chemical Biology, *Front. Chem.* **2019**, *7*, 619. (b) Yin, H.; Bardelang, D.; Wang, R. Macrocycles and Related Hosts as Supramolecular Antidotes, *Trends Chem.* **2021**, *3*, 1–4. (c) Isaacs, L. Stimuli Responsive Systems Constructed Using Cucurbit[n]uril-Type Molecular Containers, *Acc. Chem. Res.* **2014**, *47*, 2052–2062. (d) Yin, H.; Wang, R.; Applications of Cucurbit[n]urils (n=7 or 8) in Pharmaceutical Sciences and Complexation of Biomolecules, *Isr. J. Chem.* **2018**, *58*, 188–198.
- (9) (a) Logsdon, L. A.; Schardon, C. L.; Ramalingam, V.; Kwee, S. K.; Urbach, A. R. Nanomolar Binding of Peptides Containing Non-canonical Amino Acids by a Synthetic Receptor. *J. Am. Chem. Soc.* **2011**, *133*, 17087–17092. (b) Fernandes, R. J.; Remón, P.; Moro, A. J.; Seco, A.; Ferreira, A. S. D.; Pischel, U.; Basílio, N. Toward Light-Controlled Supramolecular Peptide Dimerization, *J. Org. Chem.* **2021**, *86*, 8472–8478.
- (10) (a) Chinai, J. M.; Taylor, A. B.; Ryno, L. M.; Hargreaves, N.; Morris, C. A.; Hart, P. J.; Urbach, A. R. Molecular Recognition of Insulin by a Synthetic Receptor. *J. Am. Chem. Soc.* **2011**, *133*, 8810–8813. (b) Guagnini, F.; Antonik, P. M.; Rennie, M. L.; O'Byrne, P.; Khan, A. R.; Pinalli, R.; Dalcanale, E.; Crowley, P. B. Cucurbit[7]uril-Dimethyllysine Recognition in a Model Protein, *Angew. Chem. Int. Ed.* **2018**, *57*, 7126–7130.
- (11) (a) Hennig, A.; Bakirci, H.; Nau, W. M.; Label-free continuous enzyme assays with macrocycle-fluorescent dye complexes, *Nat. Methods* **2007**, *4*, 629–632. (b) Nau, W. M.; Ghale, G.; Hennig, A.; Bakirci, H.; Bailey, D. M. Substrate-Selective Supramolecular Tandem Assays: Monitoring Enzyme Inhibition of Arginase and Diamine Oxidase by Fluorescent Dye Displacement from Calixarene and Cucurbituril Macrocycles, *J. Am. Chem. Soc.* **2009**, *131*, 11558–11570.
- (12) (a) Yang, X.; Wang, Z.; Niu, Y.; Chen, X.; Lee, S. M. Y.; Wang, R. Influence of supramolecular encapsulation of camptothecin by cucurbit[7]uril: reduced toxicity and preserved anti-cancer activity, *Med. Chem. Commun.* **2016**, *7*, 1392–1397. (b) Chen, Y.; Huang, Z.; Zhao, H.; Xu, J.-F.; Sun, Z.; Zhang, X. Supramolecular Chemotherapy: Cooperative Enhancement of Antitumor Activity by Combining Controlled Release of Oxaliplatin and Consuming of Spermine by Cucurbit[7]uril, *ACS Appl. Mater. Interfaces* **2017**, *9*, 8602–8608. (c) Appel, E. A.; Rowland, M. J.; Loh, X. J.; Heywood, R. M.; Watts, C.; Scherman, O. A. Enhanced stability and activity of temozolomide in primary glioblastoma multiforme cells with cucurbit[n]uril, *Chem. Commun.* **2012**, *48*, 9843–9845.
- (13) (a) El Maghraby, G. M.; Arafa, M. F. Liposomes for Enhanced Cellular Uptake of Anticancer Agents, *Curr. Drug Deliv.* **2020**, *17*, 861–873. (b) Lee, S.; Kim, J.; Shim, G.; Kim, S.; Han, S. E.; Kim, K.; Kwon, I. C.; Choi, Y.; Kim, Y. B.; Kim, C.-W.; Oh, Y.-K. Tetraiodoacetic acid-tagged liposomes for enhanced delivery of anticancer drug to tumor tissue via integrin receptor, *J. Control. Release* **2012**, *164*, 213–220.
- (14) Cao, L.; Hettiarachchi, G.; Briken, V.; Isaacs, L. Cucurbit[7]uril Containers for Targeted Delivery of Oxaliplatin to Cancer Cells, *Angew. Chem. Int. Ed.* **2013**, *52*, 12033–12037.
- (15) (a) Webber, M. J.; Appel, E. A.; Vinciguerra, B.; Cortinas, A. B.; Thapa, L. S.; Jhunjhunwala, S.; Isaacs, L.; Langer, R.; Anderson, D. G. Supramolecular PEGylation of biopharmaceuticals, *Proc. Natl. Acad. Sci. USA* **2016**, *113*, 14189–14194. (b) Gao, C.; Cheng, Q.; Li, J.; Chen, J.; Wang, Q.; Wei, J.; Huang, Q.; Lee, S. M. Y.; Gu, D.; Wang, R. Supramolecular Macrophage-Liposome Marriage for Cell-Hitchhiking Delivery and Immunotherapy of Acute Pneumonia and Melanoma, *Adv. Funct. Mat.* **2021**, *31*, 2102440.
- (16) (a) Gong, B.; Choi, B.-K.; Kim, J.-Y.; Shetty, D.; Ko, Y. H.; Selvapalam, N.; Lee, N. K.; Kim, K. High Affinity Host–Guest FRET Pair for Single-Vesicle Content-Mixing Assay: Observation of Flickering Fusion Events, *J. Am. Chem. Soc.* **2015**, *137*, 8908–8911. (b) Bockus, A. T.; Smith, L. C.; Grice, A. G.; Ali, O. A.; Young, C. C.; Mobley, W.; Leek, A.; Roberts, J. L.; Vinciguerra, B.; Isaacs, L.; Urbach, A. R. Cucurbit[7]uril-Tetramethylrhodamine Conjugate for Direct Sensing and Cellular Imaging. *J. Am. Chem. Soc.* **2016**, *138*, 16549–16552. (c) Li, M.; Lee, A.; Kim, S.; Shrinidhi, A.; Park, K. M.; Kim, K. Cucurbit[7]uril-conjugated dyes as live cell imaging probes: investigation on their cellular uptake and excretion pathways, *Org. Biomol. Chem.* **2019**, *17*, 6215–6220. (d) Zhang, S.; Assaf, K. I.; Huang, C.; Hennig, A.; Nau, W. M.; Ratiometric DNA sensing with a host–guest FRET pair, *Chem. Commun.* **2019**, *55*, 671–674.
- (17) (a) Zhou, X.; Su, X.; Pathak, P.; Vik, R.; Vinciguerra, B.; Isaacs, L.; Jayawickramarajah, J. Host–Guest Tethered DNA Transducer: ATP Fueled Release of a Protein Inhibitor from Cucurbit[7]uril, *J. Am. Chem. Soc.* **2017**, *139*, 13916–13921. (b) Pandey, S.; Kankanamalage, D. V. D. W.; Zhou, X.; Hu, C.; Isaacs, L.; Jayawickramarajah, J.; Mao, H. Chaperone-Assisted Host–Guest Interactions Revealed by Single-Molecule Force Spectroscopy, *J. Am. Chem. Soc.* **2019**, *141*, 18385–18389.
- (18) Yoon, D. J.; Liu, C. T.; Quinlan, D. S.; Nafisi, P. M.; Kamei, D. T. Intracellular trafficking considerations in the development of natural ligand–drug molecular conjugates for cancer, *Ann. Biomed. Eng.* **2011**, *39*, 1235–1251.
- (19) (a) Na'il Saleh Dr., Apurba L. Koner, Werner M. Nau Prof. Dr. Activation and Stabilization of Drugs by Supramolecular pKa Shifts: Drug-Delivery Applications Tailored for Cucurbiturils, *Angew. Chem. Int. Ed.* **2008**, *47*, 5398–5401. (b) Wang, R.; Yuan, L.; Macartney, D. H. A green to blue fluorescence switch of protonated 2-aminoanthracene upon inclusion in cucurbit[7]uril, *Chem. Commun.* **2005**, 5867–5869.
- (20) Malcor, J.-D.; Payrot, N.; David, M.; Faucon, A.; Abouzid, K.; Jacquot, G.; Floquet, N.; Debarbieux, F.; Rougon, G.; Martinez, J.; Khrestchatsky, M.; Vlieghe, P.; Lisowski, V. Chemical Optimization of New Ligands of the Low-Density Lipoprotein Receptor as Potential Vectors for Central Nervous System Targeting, *J. Med. Chem.* **2012**, *55*, 2227–2241.
- (21) (a) Varini, K.; Lécorché, P.; Sonnette, R.; Gassiot, F.; Broc, B.; Godard, M.; David, M.; Faucon, A.; Abouzid, K.; Ferracci, G.; Tamsamani, J.; Khrestchatsky, M.; Jacquot, G. Target engagement and intracellular delivery of mono- and bivalent LDL receptor-binding peptide-cargo conjugates: Implications for the rational design of new targeted drug therapies, *J. Control. Release* **2019**, *314*, 141–161. (b) David, M.; Lécorché, P.; Masse, M.; Faucon, A.; Abouzid, K.; Gaudin, N.; Varini, K.; Gassiot, F.; Ferracci, G.; Jacquot, G.; Vlieghe, P.; Khrestchatsky, M. Identification and characterization of highly versatile peptide-vectors that bind non-competitively to the low-density lipoprotein receptor for in vivo targeting and delivery of small molecules and protein cargos, *PLoS One* **2018**, *13*, e0191052.
- (22) (a) Brown, M. S.; Goldstein, J. L. Receptor-mediated endocytosis: insights from the lipoprotein receptor system, *Proc. Natl. Acad. Sci. USA* **1979**, *76*, 3330–3337. (b) Fong, L. G.; Bonney, E.; Kosek, J. C.; Cooper, A. D. Immunohistochemical localization of low density lipoprotein receptors in adrenal gland, liver, and intestine, *J. Clin. Invest.* **1989**, *84*, 847–856. (c) Dunn, K. W.; McGraw, T. E.; Maxfield, F. R. Iterative fractionation of recycling receptors from lysosomally destined ligands in an early sorting endosome, *J. Cell Biol.* **1989**, *109*, 3303–3314.
- (23) (a) Firestone, R. A.; Pisano, J. M.; Falck, J. R.; McPhaul, M. M.; Krieger, M. Selective delivery of cytotoxic compounds to cells by the LDL pathway, *J. Med. Chem.* **1984**, *27*, 1037–1043. (b) Vasseur, S.; Guillaumont, F. LDL Receptor: An open route to feed pancreatic tumor cells, *Mol. Cell Oncol.* **2016**, *3*, e1033586. (c) Acier, A.; Godard, M.; Gassiot, F.; Finetti, P.; Rubis, M.; Nowak, J.; Bertucci, F.; Iovanna, J. L.; Tomasini, R.; Lécorché, P.; Jacquot, G.; Khrestchatsky, M.; Tamsamani, J.; Malicet, C.; Vasseur, S.; Guillaumont, F. LDL receptor-peptide conjugate as in vivo tool for specific targeting of pancreatic ductal adenocarcinoma, *Commun. Biol.* **2021**, *4*, 987.
- (24) Jacquot, G.; Lécorché, P.; Malcor, J.-D.; Laurencin, M.; Smirnova, M.; Varini, K.; Malicet, C.; Gassiot, F.; Abouzid, K.; Faucon, A.; David, M.; Gaudin, N.; Masse, M.; Ferracci, G.; Dive, V.; Cisternino,

- S.; Khrestchatsky, M. Optimization and in Vivo Validation of Peptide Vectors Targeting the LDL Receptor, *Mol. Pharmaceutics* **2016**, *13*, 4094–4105.
- (25) Li, M.; Kim, S.; Lee, A.; Shrinidhi, A.; Ko, Y. H.; Lim, H. G.; Kim, H. H.; Bae, K. B.; Park, K. M.; Kim, K. Bio-orthogonal Supramolecular Latching inside Live Animals and Its Application for in Vivo Cancer Imaging, *ACS Appl. Mater. Interfaces* **2019**, *11*, 43920–43927.
- (26) Ayhan, M. M.; Karoui, H.; Hardy, M.; Rockenbauer, A.; Charles, L.; Rosas, R.; Udachin, K.; Tordo, P.; Bardelang, D.; Ouari, O. Comprehensive synthesis of monohydroxy-cucurbit[n]urils (n = 5, 6, 7, 8): high purity and high conversions, *J. Am. Chem. Soc.* **2015**, *137*, 10238–10245.
- (27) Ayhan, M. M.; Karoui, H.; Hardy, M.; Rockenbauer, A.; Charles, L.; Rosas, R.; Udachin, K.; Tordo, P.; Bardelang, D.; Ouari, O. Correction to “Comprehensive Synthesis of Monohydroxy-Cucurbit[n]urils (n = 5, 6, 7, 8): High Purity and High Conversions”, *J. Am. Chem. Soc.* **2016**, *138*, 6, 2060.
- (28) (a) Zhang, S.; Dominguez, Z.; Assaf, K. I.; Nilam, M.; Thiele, T.; Pischel, U.; Schedler, U.; Nau, W. M.; Hennig, A. Precise supramolecular control of surface coverage densities on polymer micro- and nanoparticles, *Chem. Sci.* **2018**, *9*, 8575–8581. (b) Chen, J.; Li, S.; Wang, Z.; Pan, Y.; Wei, J.; Lu, S.; Zhang, Q.-W.; Wang, L.-H.; Wang, R. Synthesis of an AIEgen functionalized cucurbit[7]uril for subcellular bioimaging and synergistic photodynamic therapy and supramolecular chemotherapy, *Chem. Sci.* **2021**, *12*, 7727–7734.
- (29) Moghaddam, S.; Yang, C.; Rekharsky, M.; Ko, Y. H.; Kim, K.; Inoue, Y.; Gilson, M. K. New Ultrahigh Affinity Host-Guest Complexes of Cucurbit[7]uril with Bicyclo[2.2.2]octane and Adamantane Guests: Thermodynamic Analysis and Evaluation of M2 Affinity Calculations, *J. Am. Chem. Soc.* **2011**, *133*, 3570–3581.
- (30) Goldstein, J. L.; Brown, M. S.; Anderson, R. G. W.; Russell, D. W.; Schneider, W. J. Receptor-Mediated Endocytosis: Concepts Emerging from the LDL Receptor System, *Ann. Rev. Cell Biol.* **1985**, *1*, 1–39.
- (31) Rudenko, G.; Henry, L.; Henderson, K.; Ichtchenko, K.; Brown, M. S.; Goldstein, J. L.; Deisenhofer, J. Structure of the LDL Receptor Extracellular Domain at Endosomal pH, *Science* **2002**, *298*, 2353–2358.
- (32) (a) Jallinoja, V. I. J.; Carney, B. D.; Bhatt, K.; Abbriano, C. H.; Schlyer, D. J.; Yazaki, P. J.; Houghton, J. L. Investigation of Copper-64-Based Host-Guest Chemistry Pretargeted Positron Emission Tomography, *Mol. Pharmaceutics* **2022**, *19*, 2268–2278. (b) Jallinoja, V. I. J.; Carney, B. D.; Zhu, M.; Bhatt, K.; Yazaki, P. J.; Houghton, J. L. Cucurbituril-Ferrocene: Host-Guest Based Pretargeted Positron Emission Tomography in a Xenograft Model, *Bioconjugate Chem.* **2021**, *32*, 1554–1558.
- (33) Sasmal, R.; Saha, N. D.; Pahwa, M.; Rao, S.; Joshi, D.; Inamdar, M. S.; Sheeba, V.; Agasti, S. S. Synthetic Host-Guest Assembly in Cells and Tissues: Fast, Stable, and Selective Bioorthogonal Imaging via Molecular Recognition, *Anal. Chem.* **2018**, *90*, 11305–11314.
- (34) Brown, M. S.; Goldstein, J. L.; A Receptor-Mediated Pathway for Cholesterol Homeostasis, *Science* **1986**, *232*, 34–47.
- (35) Acier, A.; Godard, M.; Gassiot, F.; Finetti, P.; Rubis, M.; Nowak, J.; Bertucci, F.; Iovanna, J. L.; Tomasini, R.; Lécorché, P.; Jacquot, G.; Khrestchatsky, M.; Tamsamani, J.; Malicet, C.; Vasseur, S.; Guillaumond, F. LDL receptor-peptide conjugate as in vivo tool for specific targeting of pancreatic ductal adenocarcinoma, *Commun. Biol.* **2021**, *4*, 987.
- (36) Liu, H.-K.; Lin, F.; Yu, S.-B.; Wu, Y.; Lu, S.; Liu, Y.-Y.; Qi, Q.-Y.; Cao, J.; Zhou, W.; Li, X.; Wang, H.; Zhang, D.-W.; Li, Z.-T.; Ma, D. Highly Water-Soluble Cucurbit[8]uril Derivative as a Broad-Spectrum Neuromuscular Block Reversal Agent, *J. Med. Chem.* **2022**, *65*, 16893–16901.
- (37) (a) Mao, D.; Liang, Y.; Liu, Y.; Zhou, X.; Ma, J.; Jiang, B.; Liu, J.; Ma, D. Acid-Labile Acyclic Cucurbit[n]uril Molecular Containers for Controlled Release, *Angew. Chem. Int. Ed.* **2017**, *56*, 12614–12618. (b) Mao, W.; Mao, D.; Yang, F.; Ma, D. Transformative Supramolecular Vesicles Based on Acid-Degradable Acyclic Cucurbit[n]uril and a Prodrug for Promoted Tumoral-Cell Uptake, *Chem. Eur. J.* **2019**, *25*, 2272–2280.
- (38) Bardelang, D.; Udachin, K. A.; Leek, D. M.; Margeson, J. C.; Chan, G.; Ratcliffe, C. I.; Ripmeester, J. A. Cucurbit[n]urils (n = 5–8): A Comprehensive Solid State Study, *Cryst. Growth Des.* **2011**, *11*, 5598–5614.
- (39) Ahn, Y.; Jang, Y.; Selvapalam, N.; Yun, G.; Kim, K. Supramolecular Velcro for Reversible Underwater Adhesion, *Angew. Chem. Int. Ed.* **2013**, *52*, 3140–3144.
- (40) Koc, A.; Khan, R.; Tuncel, D. “Clicked” Porphyrin-Cucurbituril Conjugate: A New Multifunctional Supramolecular Assembly Based on Triglycosylated Porphyrin and Monopropargyloxycucurbit[7]uril, *Chem. Eur. J.* **2018**, *24*, 15550–15555.

Table of Contents Graphic

